Article

Chinese Science Bulletin

Physical Chemistry

August 2013 Vol.58 No.24: 2950–2955
doi: 10.1007/s11434-013-5845-8

Property variation of ionic liquid [Bmim][$AuCl_4$] immobilized on carboxylated polystyrene submicrospheres with a small surface area

HE YaXing[1,3], FU HaiYing[1], LI Cheng[1], JI Xiang[2], GE XueWu[2], ZOU Yang[1], JIANG Zheng[1], XU HongJie[1] & WU GuoZhong[1*]

[1] *Shanghai Institute of Applied Physics, Chinese Academy of Sciences, Shanghai 201800, China;*
[2] *Chinese Academy of Sciences Key Laboratory of Soft Matter Chemistry, Department of Polymer Science and Engineering, University of Science and Technology of China, Hefei 230026, China;*
[3] *Graduate University of Chinese Academy of Sciences, Beijing 100049, China*

Received January 25, 2013; accepted March 18, 2013; published online May 17, 2013

In order to understand the effect of surface chemical groups on the immobilized species, Au-containing imidazolium-based ionic liquid (IL) [Bmim][$AuCl_4$] was intentionally immobilized on polystyrene (PS) submicrospheres (d ~300 nm) with a very small surface area (4–10 m^2/g), which possess carboxyl-moiety (COONa or COOH) on the surface. The behavior of immobilized [Bmim][$AuCl_4$] on the two types of submicrospheres was investigated by transmission electron microscopy (TEM), differential scanning calorimetry (DSC), and powder X-ray diffraction (XRD). It was revealed that the melting points (T_m) of [Bmim][$AuCl_4$] that had been immobilized on PS-COONa and PS-COOH submicrospheres were decreased by 2.7 and 4.1°C, respectively. The interaction mechanism between the IL and submicrosphere surface moieties was further analyzed by X-ray absorption fine structure (XAFS) analysis. The data indicated that the coordination environment of Au species changed markedly when [Bmim][$AuCl_4$] was immobilized on the surfaces of PS-COONa and PS-COOH submicrospheres, as illustrated by the decrease in white line peak intensity. The effect of surface COOH groups on T_m depression and the white line peak intensity of the XANES spectrum is more pronounced than that of COONa groups, most likely due to the possible hydrogen bond formation between the COOH group and $[Bmim]^+$.

ionic liquid, polystyrene submicrospheres, immobilization, phase behavior, XAFS

Citation: He Y X, Fu H Y, Li C, et al. Property variation of ionic liquid [Bmim][$AuCl_4$] immobilized on carboxylated polystyrene submicrospheres with a small surface area. Chin Sci Bull, 2013, 58: 2950–2955, doi: 10.1007/s11434-013-5845-8

The phase behavior or property variation of ionic liquids (ILs) immobilized on nanoparticle surfaces has been reported in the literature for SiO_2, activated carbon, etc [1–3]. Immobilized ILs were found to be more active than bulk ones. Sasaki et al. [4] prepared a series of immobilized metal ion-containing ILs on a silica surface to obtain an active and reusable catalyst for adding Kharasch between CCl_4 and styrene. Several reports have revealed T_m depression of ILs that have been immobilized onto solid surfaces. Many factors such as matrix pore size, surface functionalization and type of ILs used can affect the amount of T_m depression. Kanakubo et al. [5] found that T_m depression was dependent on pore size and that melting points were depressed as much as 30°C when the ILs [Bmim] [CF_3SO_3] and [Bmim] [$(CF_3SO_2)_2N$] were confined within CPGs. Singh et al. [6] reported the phase behavior change and a significant T_m depression ($\Delta T_m \approx -52$°C) of an imidazolium-based IL with a large anion ([Bmim][$OcSO_4$]) in a nanoporous silica gel matrix. Recently, we have investigated the phase transformation of ILs on the surface of mica [7], graphite [8] and silica nanoparticles [9] and we found that T_m of the immobilized ILs changed significantly in comparison with the bulk. For example, Liu et al. [9] immobilized four types of imidazolium-based ILs onto the surface of SiOx nanoparticles

*Corresponding author (email: wuguozhong@sinap.ac.cn)

(d ~20 nm) and found that the T_m of the immobilized ILs was depressed significantly compared to bulk ILs.

Although the specific surface area of nanoparticle has an important role in controlling the behavior of immobilized ILs, surface chemistry may also play an important role via hydrogen bonding or electrostatic interaction between surface groups and immobilized ILs. In this work, we employed polystyrene submicrospheres (PS) as substrates to investigate the effect of surface chemistry on the phase behavior of an IL. Polystyrene submicrospheres were functionalized with carboxylic acid groups to possess negative surface charge. Compared to the nanoparticles in a size of d ~20 nm whose surface area is about 640 m^2/g, the surface area of PS submicrospheres used in this work is 9.29 m^2/g (d ~300 nm) which is smaller by three orders of magnitude. Therefore, the particle size effect on the immobilized ILs can be ignored. We immobilized the IL [Bmim][$AuCl_4$] on the surface of carboxylic acid group functionalized polystyrene submicrospheres through physisorption. Attention was paid to the effect of submicrosphere surface chemistry on the T_m depression and structure variation of [Bmim][$AuCl_4$]. The structure of the immobilized ILs were characterized by X-ray absorption fine structure (XAFS). Although many studies have been performed on immobilized ion-containing IL, XAFS is rarely applied for this purpose. In this study, [Bmim][$AuCl_4$] was chosen because its L-edge spectra relating to the density of d states can be used to estimate the oxidation states of active sites in the target atom. XAFS was used to analyze the structural transformation of immobilized [Bmim][$AuCl_4$] to elucidate the changes in the coordination environment of Au when the IL was immobilized on the surface of polystyrene submicrospheres that had been functionalized as described above. The behavior of immobilized IL was also measured by differential scanning calorimetry (DSC) and other techniques.

1 Experimental

1.1 Materials

All the materials were reagent grade and used as purchased. Polystyrene submicrospheres functionalized by carboxylic group (mean diameter of 310 nm) were prepared by a method previously described in the literature [10]. PS submicrospheres that have carboxyl moieties were synthesized via a two-step dispersion polymerization in an ethanol-water mixture using polyvinyl pyrrolidone (PVP) as a dispersant. Then, the PS submicrospheres were prepared following the itaconic acid (ITA) variant prep, maintaining all the same ingredients. A 250 mL four-necked vessel was charged with the mixtures containing 5.0 g styrene, 0.10 g 2,2-azobisisobutyronitrile, 2.0 g PVP, 0.1 g ITA, 4 g water, and 76 g ethanol. The reaction system was deoxygenated by bubbling with nitrogen gas for approximately 30 min at room temperature. Then the polymerization reaction took place when the temperature increased up to 75°C. Carboxylated PS submicrospheres were obtained after the polymerization was performed for 3.5 h (named PS-COOH submicrosphere for simplicity).

[Bmim][$AuCl_4$] was synthesized according to a method previously described in the literature [11]. A slight excess of [Bmim]Cl (0.13 g, 0.74 mmol) was added to tetrachloroauric acid ($HAuCl_4 \cdot 4H_2O$, 0.275 g, 0.67 mmol) to instantly form a soft yellow solid. The reaction was completed by gently stirring heated water bath, just above the melting point of [Bmim][$AuCl_4$]. This solution was purified by recrystallization from a 4∶1 benzene∶acetonitrile solution. The specific surface area of PS-COOH was about 9.29 m^2/g characterized by Brunauer Emmett Teller (BET) method and the carboxyl contents on the surface of PS-COOH was 0.202 mmol/g determined by conductometric titration using the aqueous solution of NaOH.

1.2 Sample preparation

To negatively charge the surface, the PS-COOH submicrospheres were neutralized with sodium hydroxide, and the as-obtained samples were called PS-COONa. Its specific surface area was 4.19 m^2/g characterized by BET method which is a half of the PS-COOH submicrospheres. The immobilized ILs were prepared by adding [Bmim][$AuCl_4$] and functionalized PS to an appropriate amount of ethanol solution. This solution was constantly stirred for 24 h and then dried at 60°C in a vacuum for 24 h to remove the ethanol. These two samples were abbreviated as [Bmim][$AuCl_4$]/PS-COOH and [Bmim][$AuCl_4$]/PS-COONa, respectively. The loading amounts of the [Bmim][$AuCl_4$] on the two functional PS were estimated to be 42% by thermal gravity analysis.

1.3 Methods

The phase transition temperatures of bulk and immobilized ILs were measured by DSC (DSC-822e, Mettler-Toledo Corp). Samples (approximately 10 mg) were placed in aluminum pans with pierced lids. The temperature was scanned from 0 to 100°C at a programmed rate of 10°C/min. The liquid nitrogen cooling system in the DSC equipment was used to cool the sample from room temperature to 0°C.

The XAFS measurement was carried out at the 14 W beam line of Shanghai Synchrotron Radiation Facility. During the measurement, the synchrotron acceperator was operated at an energy of 3.5 GeV and a current between 150 and 210 mA. The station was operated with a Si(111) double crystal monochromator. The X-ray absorption data at the Au L3-edge of the samples were recorded at room temperature in transmission mode using ion chambers. The photon energy was calibrated with the first inflection point of Au L3-edge in platinum metal foil.

X-ray diffraction (XRD) patterns were recorded with a

Philips X-ray diffractometer (PW-1710) using Cu Kα radiation ranging from 5° to 60° (2θ). XRD patterns of PS with and without IL have been recorded.

Transmission electron microscopy (TEM) was performed on a Zeiss EM 912 operated at 120 kV. The samples were ground in an agate mortar and suspended in acetone. One drop of the suspension was deposited on a carbon-coated copper grid. Then the sample was allowed to dry for 10 min before microscopic examination.

2 Results and discussion

2.1 Morphology comparison and phase behavior change

The morphology of prepared PS-COOH microspheres is shown in Figure 1, indicating the mean diameter of the sample was about 300 nm. When [Bmim][$AuCl_4$] is immobilized to PS-COOH microspheres, the images have higher resolution, as shown in Figure 2. The crystalline clusters are clearly observed on the surface of the functionalized polystyrene submicrospheres. The arrows in the TEM micrographs imply that the clusters have various crystalline orientations and exist randomly on the submicrosphere surface.

To determine the effect of immobilization on the T_m of the IL, DSC experiments were conducted. Figure 3 shows DSC curves for bulk and immobilized [Bmim][$AuCl_4$] samples. The T_m of bulk [Bmim][$AuCl_4$] was measured to be 61°C, which was slightly different from the literature [11]. This difference may be due to the different measurement methods applied. Upon immobilization on the PS-COONa submicropheres, T_m of the IL is 58.3°C, which is 2.7°C lower than the bulk IL. In comparison, when immobilized on the PS-COOH submicrospheres, T_m is 56.9°C, which is 4.1°C lower than the bulk IL. Our results are in good agreement with the reports [5,9,12–14] in which a significant T_m depression is also observed when ILs are immobilized or confined to the solid surfaces. However, the degree of depression in this work is lower than previously reported values, most likely due to the much larger diameter of the submicrospheres and different surface groups used in this study.

The change in T_m upon immobilization can be explained in terms of the interactions between the IL and the submicrosphere surface in a manner similar to that suggested by previous reports concerning molecules confined in mesoporous silica [15] and nanospheres [16]. The degree of depression of the melting point (ΔT_m) is dependent on interfacial interactions between the IL and the submicrosphere surfaces. In the case of [Bmim][$AuCl_4$]/PS-COONa, there are interactions at the interface (intermolecular interactions) and the electrostatic interaction between $[Bmim]^+$ (from [Bmim][$AuCl_4$]) and $PS\text{-}COO^-$. The strong van der Waals interactions (intermolecular interactions) between the immobilized ILs and the PS-COONa submicrospheres will decrease the mobility of IL cations near the interface because the cations prefer to adsorb onto the PS-COONa submicrospheres. Consequently, the cations are trapped in a higher-entropy state, leading to a reduction in T_m. In comparison, the electrostatic interaction between immobilized IL and PS-COONa will presumably increase the T_m of the IL (Scheme 1, bottom). The combination of these two factors results in a lower T_m compared to the bulk IL. However, in the case of [Bmim][$AuCl_4$]/PS-COOH, the hydrogen-bond network formed by

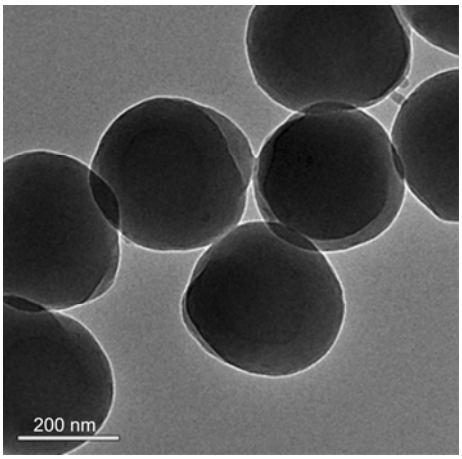

Figure 1 TEM image of the carboxylated functionalized PS-COOH.

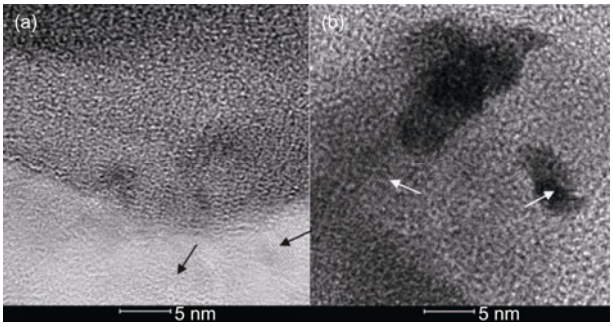

Figure 2 TEM images of [Bmim][$AuCl_4$]/PS-COOH (a) and [Bmim][$AuCl_4$]/PS-COONa (b). The arrows show the existence of crystalline clusters on the submicrosphere surface.

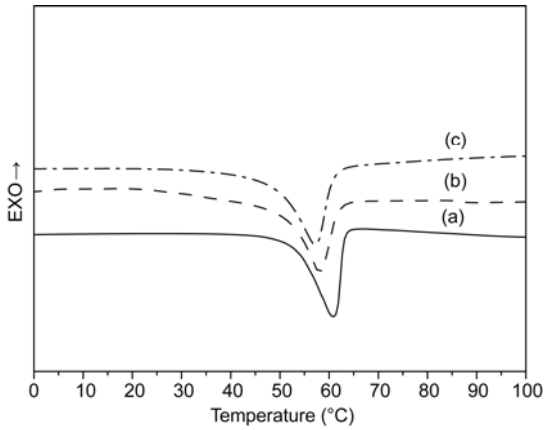

Figure 3 DSC traces of [Bmim][$AuCl_4$] (a), [Bmim][$AuCl_4$]/PS-COONa (b), and [Bmim][$AuCl_4$] /PS-COOH (c).

the surface carboxyl groups may affect the T_m. H-bonding can also lead to an increase in the T_m of IL, but the H-bonding is usually weaker than the electrostatic interaction. Hence, the cumulative interactions between [Bmim][$AuCl_4$] and the PS-COOH submicrosphere surface led to a lower T_m of [Bmim][$AuCl_4$]/PS-COOH compared to the bulk IL and the [Bmim][$AuCl_4$]/PS-COONa. On the other hand, thermal gravity and FT-IR methods were further used to compare the properties after the immobilization of IL. The decomposition point for [Bmim][$AuCl_4$]/PS-COOH and [Bmim][$AuCl_4$]/PS-COONa both decreased by 35°C. Moreover, no new peak was observed from FT-IR spectra, indicating no chemical bond between the IL and PS-COOH or PS-COONa microsphere (data not shown). Therefore, the possible immobilizing mechanism is assumed as Scheme 1.

2.2 Structural characterization by XAFS and XRD

XAFS analysis is a useable method to reveal the local structural information at the atomic scale. Figure 4 shows XAFS spectra of Au species in [Bmim][$AuCl_4$] (a), [Bmim][$AuCl_4$]/PS-COONa (b), and [Bmim][$AuCl_4$]/PS-COOH (c). The XAFS spectra of three samples are very similar, indicating that the coordination shells and atoms around Au are similar. Because X-ray absorption near edge structure (XANES) spectra are more sensitive to the change in the Au inner coordination sphere, Figure 5 further shows XANES spectra of Au species in three different samples. It displays intense edge resonance positions at 11920 eV due to an electronic transition from a 2p core state to an empty 5d final state [17,18]. The white line peak of the immobilized Au-containing ILs is clearly lower than that of bulk IL; simultaneously, the white line peak intensity of [Bmim][$AuCl_4$]/PS-COOH is lower than that of [Bmim][$AuCl_4$]/PS-COONa. This finding implies that the coordination environment of Au species varies noticeably when the [Bmim][$AuCl_4$] is immobilized on the surface of PS submicrospheres. In agreement with the DSC measurement, the T_m of [Bmim][$AuCl_4$] immobilized on the PS-COOH submicrospheres is lower than both that of the bulk IL and of that immobilized on the PS-COONa submicrospheres. These results are in good agreement with the report by Tanaka et al. [18] who observed the formation of gold nanoparticles prepared by $NaBH_4$ reduction of Au^{3+} in toluene in the presence of dodecanethiol (DT) and found that, when Au^{3+} was reduced to Au^{+} or even to Au, the white line became weaker, and finally disappeared.

The change in white line peak intensity of immobilized ILs can be interpreted as the variation in the electron density of Au atom in [Bmim][$AuCl_4$]. The decrease of the white line peak intensity is attributed to an increase in the 5d occupancy of the Au atom [18,19]. For [Bmim][$AuCl_4$]/PS-COOH, the anion of the IL forms hydrogen bonds with carboxylic acid moieties that are attached to the polystyrene submicrospheres. Thus, the electron cloud of oxygen in the carboxylic acid moiety transfers to the $AuCl_4^-$, and the electron density of the Au atom is increased. In the case of [Bmim][$AuCl_4$]/PS-COONa, the obtained lower white line peak intensity may be caused by the partial transfer of negative charge of the surface –COONa groups to the anion of the IL. However, due to the electrostatic repulsion between PS-COO^- and $AuCl_4^-$, the increase in electron density of the Au atom in [Bmim][$AuCl_4$]/PS-COONa is less than that of

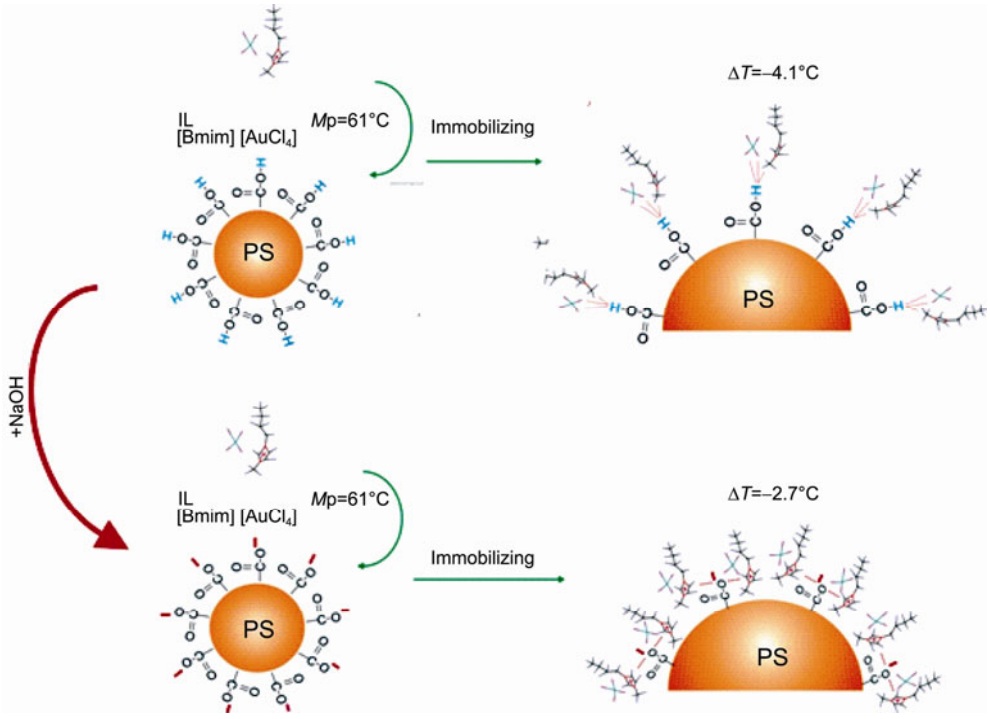

Scheme 1 Schematic diagram of IL [Bmim][$AuCl_4$] immobilized on two different functional polystyrene microspheres.

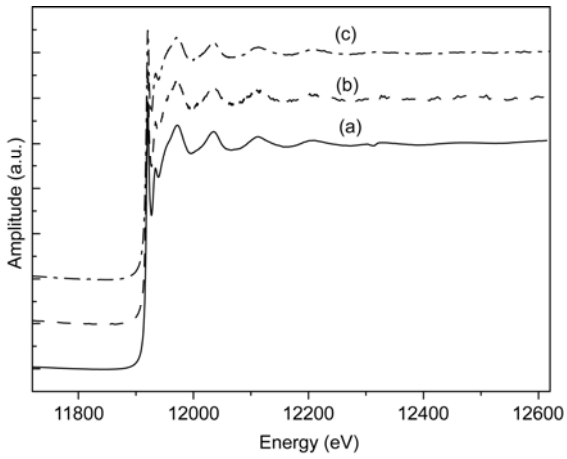

Figure 4 XAFS spectra of Au species in [Bmim][$AuCl_4$] (a), [Bmim][$AuCl_4$]/PS-COONa (b), and [Bmim][$AuCl_4$]/PS-COOH (c).

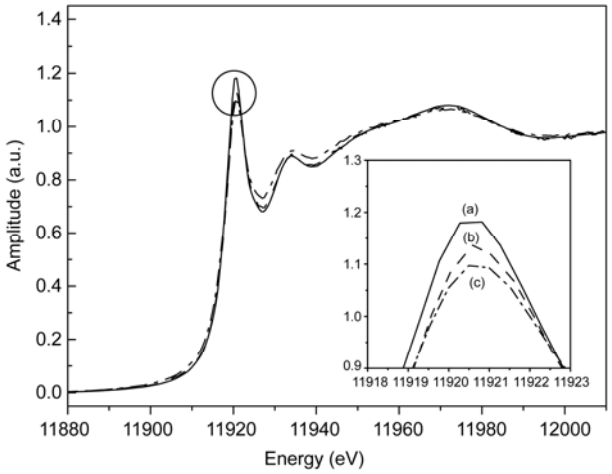

Figure 5 XANES spectra of Au species in [Bmim][$AuCl_4$] (a), [Bmim][$AuCl_4$]/PS-COONa (b), and [Bmim][$AuCl_4$]/PS-COOH (c).

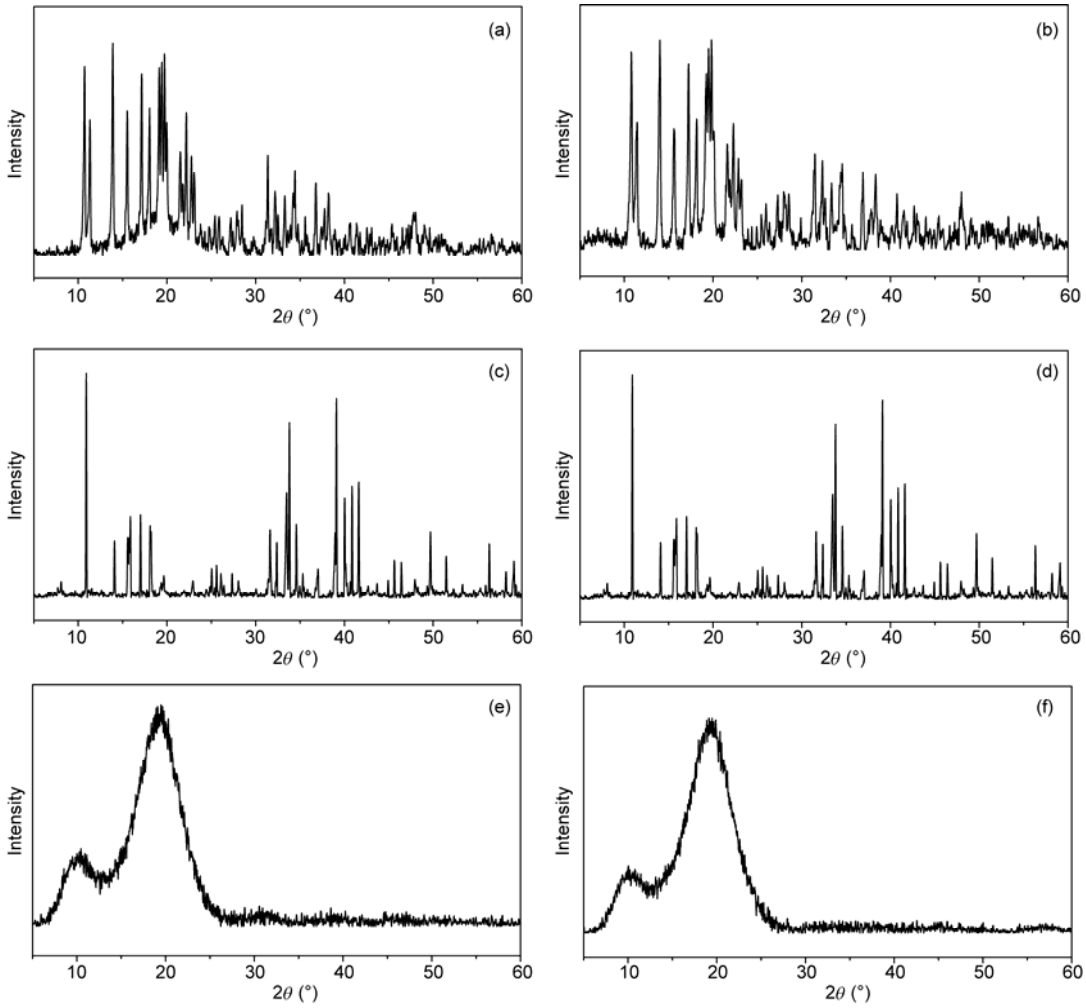

Figure 6 XRD diffractograms for [Bmim][$AuCl_4$]/PS-COONa (a), [Bmim][$AuCl_4$]/PS-COOH (b), bulk [Bmim][$AuCl_4$] (c), bulk [Bmim][$AuCl_4$] (d), PS-COONa submicrospheres (e), and PS-COOH submicrospheres (f).

[Bmim][$AuCl_4$]/PS-COOH. Consequently, the decrease in white line peak intensity of [Bmim][$AuCl_4$]/PS-COOH is of a greater magnitude.

Figure 6 shows the XRD patterns of PS submicrospheres, bulk IL and IL/submicrosphere samples. Characteristic peaks are observed for both the pure and immobilized ILs. As

shown in Figure 6, the XRD patterns indicate that the PS-COOH and PS-COONa submicrospheres are amorphous, whereas the IL has many diffraction peaks. Compared to the bulk [Bmim][$AuCl_4$], the relative intensities and theta of the XRD peaks of the immobilized ILs are significantly different. For [Bmim][$AuCl_4$]/PS-COONa (Figure 6(a)), compared to the bulk [Bmim][$AuCl_4$], new peaks appear at 2θ of 22°, 14.1°, 15.9°, 17.1°, 18.1°, etc. Relative intensities of these peaks are obviously different from those of the bulk IL. Similar phenomena were observed for the XRD analysis of [Bmim][$AuCl_4$]/PS-COOH. The XRD analysis demonstrates that the conformation or stacking of [Bmim][$AuCl_4$] after immobilization on functional polystyrene submicrospheres is changed. Interfacial and electrostatic interactions as well as hydrogen bonds most likely change the stacking pattern of immobilized [Bmim][$AuCl_4$]. This speculation is consistent with the conclusions of previous studies [20–23], in which it was proposed that the chemical bond between the IL and the solid surface limited the degrees of freedom of the dialkyl imidazolium cation and changed the structure of immobilized ILs, resulting also in an obvious variation of XRD patterns.

3 Conclusions

In the present work, [Bmim][$AuCl_4$] was successfully immobilized on PS-COONa and PS-COOH submicrospheres, and the behavior variation of IL was investigated using various methods including XAFS and thermal analysis. The results of DSC measurement showed a depression in the T_m of the immobilized IL. Moreover, the T_m of [Bmim][$AuCl_4$]/PS-COOH was lower than that of the bulk IL and [Bmim][$AuCl_4$]/PS-COONa. The XAFS analysis further indicated that the coordination environment of Au species changed markedly when the [Bmim][$AuCl_4$] was immobilized on the surface of polystyrene submicrospheres. Therefore, it was assumed that the T_m depression and structural change of the immobilized ILs were mainly due to interfacial and electrostatic interactions as well as hydrogen bonds between the IL and the submicrospheres.

This work was supported by the National Natural Science Foundation of China (11079007, 51073146, 51103143, 11005148, 20973192 and 10705046).

1 Mehnert C P. Supported ionic liquid phases. Chem Eur J, 2004, 11: 50–56
2 Wu X, Letuchy Y A, Eyman D P. Catalytic hydrodechlorination of CCl_4 over silica-supported $PdCl_2$-containing molten salt catalysts: The promotional effects of $CoCl_2$ and $CuCl_2$. J Catal, 1996, 161: 164–177
3 Sasaki T, Tada M, Zhong C M, et al. Immobilized metal ion-containing ionic liquids: Preparation, structure and catalytic performances in Kharasch addition reaction and Suzuki cross-coupling reactions. J Mol Catal A-Chem, 2008, 279: 200–209
4 Sasaki T, Zhong C M, Tada M, et al. Immobilized metal ion-containing ionic liquids: Preparation, structure and catalytic performance in Kharasch addition reaction. Chem Commun, 2005, 2506–2508
5 Kanakubo M, Hiejima Y, Minami K, et al. Melting point depression of ionic liquids confined in nanospaces. Chem Commun, 2006, 1828–1830
6 Singh M P, Singh R K, Chandra S. Studies on imidazolium-based ionic liquids having a large anion confined in a nanoporous silica gel matrix. J Phys Chem B, 2011, 115: 7505–7514
7 Liu Y D, Zhang Y, Wu G Z, et al. Coexistence of liquid and solid phases of Bmim-PF_6 ionic liquid on mica surfaces at room temperature. J Am Chem Soc, 2006, 128, 7456–7457
8 Sha M L, Zhang F C, Wu G Z, et al. Ordering layers of bmim PF_6 ionic liquid on graphite surfaces: Molecular dynamics simulation. J Chem Phys, 2008, 128: 134504
9 Liu Y S, Wu G Z, Fu H Y, et al. Immobilization and melting point depression of imidazolium ionic liquids on the surface of nano-SiO_x particles. Dalton Trans, 2010, 39: 3190–3194
10 Zhang J V, Ge X W, Wang M Z, et al. Colloidal silver deposition onto functionalized polystyrene microspheres. Polym Chem, 2011, 2: 970–974
11 Hasan M, Kozhevnikov I V, Siddiqui M R H, et al. Gold compounds as ionic liquids. Synthesis, structures, and thermal properties of *N*,*N*′-dialkylimidazolium tetrachloroaurate salts. Inorg Chem, 1999, 38: 5637–5641
12 Neouze M A, Le Bideau J, Gaveau P, et al. Ionogels, new materials arising from the confinement of ionic liquids within silica-derived networks. Chem Mater, 2006, 18: 3931–3936
13 Goebel R, Hesemann P, Weber J, et al. Surprisingly high, bulk liquid-like mobility of silica-confined ionic liquids. Phys Chem Chem Phys, 2009, 11: 3653–3662
14 Neouze M A, Litschauer M. Confinement of 1-butyl-3-methylimidazolium nitrate in metallic silver. J Phys Chem B, 2008, 112: 16721–16725
15 Trofymluk O, Levchenko A A, Navrotsky A. Interfacial effects on vitrification of confined glass-forming liquids. J Chem Phys, 2005, 123: 194509
16 Rittigstein P, Torkelson J M. Polymer-nanoparticle interfacial interactions in polymer nanocomposites: Confinement effects on glass transition temperature and suppression of physical aging. J Polym Sci B, 2006, 44: 2935–2943
17 Nishimura S, Anh T N D, Mott D, et al. X-ray absorption near-edge structure and X-ray photoelectron spectroscopy studies of interfacial charge transfer in gold-silver-gold double-shell nanoparticles. J Phys Chem C, 2012, 116: 4511–4516
18 Tanaka T, Ohyama J, Teramura K, et al. Formation mechanism of metal nanoparticles studied by XAFS spectroscopy and effective synthesis of small metal nanoparticles. Catal Today, 2012, 183: 108–118
19 Qi B, Perez I, Ansari P H, et al. L2 and L3 measurements of transition-metal 5D orbital occupancy, spin-orbit effects, and chemical bonding. Phys Rev B, 1987, 36: 2972–2975
20 Fitchett B A, Conboy J C. Structure of the room-temperature ionic liquid/SiO_2 interface studied by sum-frequency vibrational spectroscopy. J Phys Chem B, 2004, 108: 20255–20262
21 Guegan R, Morineau D, Alba-Simionesco C. Interfacial structure of an H-bonding liquid confined into silica nanopore with surface silanols. Chem Phys, 2005, 317: 236–244
22 Vishweshwar P, Nangia A, Lynch V M. Molecular complexes of homologous alkanedicarboxylic acids with isonicotinamide: X-ray crystal structures, hydrogen bond synthons, and melting point alternation. Cryst Growth Des, 2003, 3: 783–790
23 Huang W, Qian H F. C-H···X hydrogen-bond-mediated supramolecular frameworks: Syntheses and crystal structures of hydrochlorate hexafluorophosphorate and hydrochlorate tetrafluoroborate of 4′-chloro-2,2′:6,2″-terpyridine. J Mol Struct, 2007, 832: 108–116